August 2013

Synthesis and Compressive Properties of Al-A206/SiC and Mg-AZ91/SiC Syntactic Foams

Gonzalo A. Rocha Rivero
University of Wisconsin-Milwaukee

SYNTHESIS AND COMPRESSIVE PROPERTIES OF Al-A206/SiC AND Mg-AZ91/SiC SYNTACTIC FOAMS

by

Gonzalo Rocha Rivero

A Thesis Submitted in

Partial Fulfillment of the

Requirements for the Degree of

Master of Science

in Engineering

at

The University of Wisconsin-Milwaukee

August 2013

ABSTRACT

SYNTHESIS AND COMPRESSIVE PROPERTIES OF Al-A206/SiC AND Mg-AZ91/SiC SYNTACTIC FOAMS

by

Gonzalo Rocha Rivero

The University of Wisconsin-Milwaukee, 2013
Under the Supervision of Professor Pradeep Rohatgi

Metal matrix syntactic foams are promising materials for energy absorption. Maximizing specific energy absorption requires a strong low density matrix and strong ceramic reinforcements. Very few studies on the use of SiC microballons in metal matrix syntactic foams have been published in the literature. The objective of this thesis was to study the effects of matrix strength on the quasistatic compressive properties of syntactic foams using SiC hollow spheres as reinforcement and Aluminum A206 and Magnesium AZ91 as matrices. The SiC hollow microspheres syntactic foams were synthesized by a sub-atmospheric pressure infiltration technique and the resulting samples were then tested in compression at a strain rate of 10^{-3} s^{-1} using a conventional load frame. The energy absorbed by syntactic foams in this study is represented by the area under the compressive stress-strain curve from the peak stress until densification again reaches the peak stress at a large strain. Because Al-A206 is a heat treatable alloy, matrix strength can be varied by heat treatment condition and foams in as-cast, T4, and T7 conditions were tested in this study. It is shown that the peak strength, plateau

strength and toughness of the foams increase with increasing yield strength of the matrix and that these foams show better performance than many syntactic foams reported in the literature, on a specific property basis.

The peak strength, plateau strength and toughness of the foams studied increase with increasing yield stress of the matrix material. The increments for the peak stress were 13% for T4 and 24% for T7 treatments, referred to the as cast condition. For the same heat treatments, the increments for the plateau stress were 27% and 37%, while for the Toughness the values were 17% and 26% respectively.

TABLE OF CONTENTS

LIST OF FIGURES

LIST OF TABLES

LIST OF ABREVIATIONS

Term	Abbreviation
Metal Matrix Syntactic Foam	MMSF
Wall Thickness/ Sphere Diameter	(t/D)
Scanning Electron Microscope	SEM
Energy Dispersive Spectroscopy	EDS
Atomic mass composition, in percentage	(at%)
Mass composition, in percentage	(wt%)
Volume composition, en percentage	(V%)
Functionally graded armor composites	FGAC
The United States Patent and Trademark Office	USPTO

ACKNOWLDGEMENTS

This research was supported by the U.S. Army-TARDEC through TACOM R&D Contract# W56HZV-08-C-0716. The views, opinions, and conclusions made in this document are those of the author and should not be interpreted as representing the official policies, either expressed or implied, of U.S. Army-TARDEC or the U.S. Government. The U.S. Government is authorized to reproduce and distribute reprints for Government purposes not withstanding any copyright notation herein. I would like to thank Dr. Rohatgi for providing me with an opportunity to do research in his and supervise my thesis. I am also deeply thankful for the help of Dr. Benjamin Schultz and Dr. J.B. Ferguson who assisted me with my research.

1. Introduction

Metal matrix syntactic foams are a type of particulate composite in which hollow microspheres are contained within a metal matrix. With this approach, porosity is added to a monolithic metal in a controlled way, to improve some of the properties of the resulting composite. Lower densities, higher energy absorption, heat insulation and sound absorption capabilities are some of the advantages of syntactic foams that have attracted the attention of industry and the academia. Regarding their energy absorption properties, syntactic foams usually have a characteristic quasi-static compression stress strain curve consisting of an initial linear region followed by a long stress plateau. The behavior in the initial region is usually considered elastic, although due to the nature of syntactic foams, with a variety of spheres sizes and wall thicknesses, this region is not truly elastic and some deviations are observed. At the end of this region a drop in the stress is produced before the stress plateau appears. The plateau region is where most of the hollow spheres crush and the composite material absorb energy without any significant change in their strength. The crushing of hollow spheres and their compaction lead to the densification of the composite material; once the densification is complete, the stress again increases steadily over the material. The energy absorbed by syntactic foams synthetized in this study is represented by the area under the compressive stress-strain curve from the peak stress until densification again reaches the peak stress at a large strain [19, 20].

Extensive research has been done on metallic syntactic foams, especially with cenospheres and alumina hollow spheres, yet few studies have been published with the use of SiC hollow spheres as reinforcement in metal matrix syntactic foams [34].

The objective of this work was to study the effects of matrix strength on the quasistatic compressive properties of syntactic foams using SiC hollow spheres as reinforcement and Aluminum A206 and Magnesium AZ91 as matrices.

2. Literature Review

2.1 Synthesis of Metal Matrix Syntactic foams

The methods used for the synthesis of metal matrix syntactic foams are basically the same as those used for the processing of metal matrix composites, though in this case the unique characteristic of the composites (hollow materials) may impose some restrictions in the use of these methods. In the following section the main processes used for the synthesis of metal matrix syntactic foams will be presented, as well as some of the problems found. The methods reported in the literature, can be divided in two approaches [1]:

- Solidification techniques, processes that involve the incorporation of the spheres in the molten metal and casting to form a shape. Pressure infiltration and stir casting are the main processes within this group.
- Powder Metallurgy, processes where the metal and the hollow spheres powders are mixed, consolidated, degasified and sintered to form a shape.

2.1.1 Pressure Infiltration

Is the most used method for processing MMSF because the metal is forced to flow through the openings and crevices between the hollow spheres, overcoming the poor wetting observed between a metal matrix and ceramic materials used as hollow spheres. The method usually comprises the preparation of a preform with the hollow reinforcements; eventually the spheres can be loosely packed. The pressure needed to infiltrate the molten metal through the crevices of the preform can be applied through an inert gas [2-7], vacuum infiltration [8-11], mechanical pressure (squeeze or die casting) [12-17].

A good adhesion between the matrix and the reinforcement is crucial for an appropriate performance of any composite material. Wettability is the ability of a liquid to spread on a solid surface [77]. A good wettability between the melt and the hollow spheres is very important for a good adhesion between these surfaces; the liquid matrix must penetrate and wet the surface of the spheres to avoid an incomplete infiltration of the reinforcement. Usually the wetting of ceramic reinforcements by liquid metals is rather poor; hence an adequate selection of the infiltration parameters or the uses of preforms are options to improve this behavior.

In the gas pressure infiltration technique, the preform is held in a mold or crucible, separated from the solid metal charge with a filter (ZrO_2 or Y_2O_3). The chamber containing the mold is degassed to remove the gas in the preform, and heated to above the melting temperature of the metal. Once the metal is completely melted, an inert gas

is applied to the chamber to force the liquid metal into the preform. Afterwards, the infiltrated syntactic foam is allowed to solidify. Pressure and temperature of the system as well as wetting at the metal/reinforcement interface and permeability of the reinforcement bed are critical factors for a complete infiltration. These parameters should be chosen carefully, to avoid an incomplete infiltration (unintended porosity in the foam). However, higher temperatures could increase the possibility of formation of undesirable phases due to a chemical reaction between the matrix and the material of the spheres; on the other hand an excessive infiltration pressure could lead to the crushing of the spheres and their filling with metal [3]. Coating the hollow spheres with metals improve the wetting between the metal matrix and the spheres, allowing the use of a reduced infiltration pressure, as shown by Rohatgi et al. [18] where the infiltration pressure was reduced from 3 and 4 psi for uncoated fly ash to around 1 psi for Ni-coated fly ash.

Vacuum infiltration is similar to gas pressure infiltration, i.e. vacuum is applied to the chamber and heat is applied until the metal is completely melted. The infiltration is achieved by applying a negative differential pressure between the metal and the hollow reinforcement with an inert gas. This approach shows advantages over the gas pressure infiltration when the hollow spheres are fragile and are damaged by high infiltration pressures. Usually this process is accomplished with the use of coatings that improve the wettability of the liquid metal and the hollow spheres. This method has been used by J. Santa Maria et al. to synthesize syntactic foams from Al-A380 and Al-A206 with Al_2O_3 hollow spheres [19-20].

Squeeze casting is an alternative method to apply the pressure needed for infiltration of hollow spheres preforms. In this process the upper part of the mold is pressed into the liquid melt forcing it to infiltrate the preform. This process presents some advantages like the ability to produce a near net shape piece, virtually free from porosity and with a finer grain size. Several researchers [12-15] have used this method to infiltrate loose spheres and preforms and get aluminum matrix syntactic foams.

2.1.2 Stir Casting

Stir casting is a technique that describes several methods where a molten metal is agitated and stirred, usually with an impeller, to disperse a reinforcing phase throughout the metal. This method is particularly sensitive to segregation and agglomeration of the hollow reinforcement, therefore the melt has to be continuously stirred before being poured into the mold. Addition of compacted pellets with the reinforcement is the most common used method for transfer of the particles to the melt. Daoud et al. have successfully used this method to processing syntactic foams made of magnesium alloy ZC63 with 12-25% fly ash [21] and ZnAl22 with Ni-coated fly ash [22].

2.1.3 Powder Metallurgy

This method has been used successfully for the processing of syntactic foams using different matrices like aluminum, iron and titanium [13, 14, 23-26, 28-30]. The powder alloy and the hollow spheres are mixed in appropriate amounts, and then the mixture is compacted under pressure into a shape and sintered in a furnace to get a near full density piece. This method has been used in the processing of many metal matrix

composites, however in the case of syntactic foams; special care should be taken in the selection of a compaction pressure that minimizes the crushing of hollow spheres. Zhao et al. synthesized Fe and Ti syntactic foams by powder metallurgy, using compaction pressures of 100 and 150 MPa and E-spheres (hollow and porous) [15]; the results obtained showed that a significant number of spheres were crushed at the higher compaction pressure. In a similar study, Xue et al. synthesized Ti-ceramic microspheres syntactic foams, using compaction pressures of 45 and 200 MPa [69]. The density and porosity of the foams varied with compaction pressure, however a higher compaction pressure resulted in a large number of crushed microspheres.

2.2 Processing Defects in Metal Matrix Syntactic Foams

The processing of syntactic foams presents some technological problems that can have negative implications on the quality of syntactic foams; usually evidenced as defects in the foams. These defects have their origin in some characteristics inherent to the physico-chemical interactions between the metal matrix and the hollow particles added as well as the processing parameters and eventually in the quality of the hollow spheres.

2.2.1 Physical and Chemical Interactions

Most of the hollow reinforcements in metal matrix syntactic foams are ceramic; the wetting between these two surfaces is not good and this condition usually leads to a poor bonding and unintended porosity localized around the hollow sphere periphery [5, 7, 31, 32]. It has been shown that unintended porosity has an adverse effect on the mechanical behavior of aluminum fly ash syntactic foams, by lowering the peak stress of

the stress-strain curve [31]. This defect becomes more critical as the size of microspheres becomes smaller due to capillary resistance to the flow of the melt through the voids between the microspheres [7]. Coating of the microspheres with metals (Al, Ag, Cu, Ni,) is an alternative that has been used to reduce unintended porosity [7]. Increasing the infiltration pressure is another option, although this also increases the possibility of infiltrating the cavity of the microspheres due to an excessive pressure.

On the other hand, high temperature and pressure conditions, usually found in the processing of syntactic foams, can lead to chemical reactions between the matrix and hollow reinforcements. These reactions depend on the particular compositions of both elements of the foam and they may affect adversely the mechanical strength of the matrix due to modifications in its chemical composition and phases, as shown by Balch et al. [27] where the aluminum melt react with the ceramic microspheres leading to the formation of solid Silicon inclusions inside the matrix and alumina over the surface of the microspheres. These changes may also have a strong influence on the heat treatment of these composites as illustrated by the work of Orbulov et al. [6].

The strength of the spheres may be also reduced by these chemical interactions due to a reduction in their wall thickness or other damage which can lead to infiltration of the spheres [4, 6, 7, 27].

2.2.2 Processing Parameters

Beside the pressure and temperature effects mentioned in the previous section, gradients in reinforcement have been found to be introduced in the foams due to interactions between the solid hollow spheres and the advancing liquid and solidification front of the matrix [7]. This effect may be adverse if the infiltration takes place through a loosely packed bed of hollow spheres because the liquid metal flow pushes and creates turbulence modifying the distribution of hollow spheres inside the foam; eventually this fact leads to non-consistent mechanical properties in the foam due to the presence of metal rich regions and regions with agglomerated hollow spheres in other ones. The use of preforms minimizes this problem when sintering or binding of the reinforcement is possible. Besides allowing more far consistent mechanical properties in metal matrix syntactic foams, preforms having a bimodal size distribution of hollow spheres may be made through this process. According to the literature, this distribution of hollow spheres could lead to an even greater enhancement of the peak stress and the plateau resistance of syntactic foams [16].

2.2.3 Quality of the Hollow spheres

Consistency in the properties of hollow spheres also plays a role in the mechanical behavior of syntactic foams. In this case the main factors involved are the size distribution of the spheres, microsphere wall thickness/diameter ratio and the amount of broken or porous microspheres. Figure 1 shows the appearance and inner surface of the most common types of microspheres reported in the literature (flyash cenosphere,

ceramic microballon (36-40% Al_2O_3, 55-60% SiO_2, 1.4-1.6%TiO_2, 0.4-0.5% Fe_2O_3) and SiC microspheres). It can be seen that microspheres are not completely spherical, their thickness is not uniform, they are porous and their inner cavities are not completely hollow. These characteristics may affect adversely the quality of MMSF and should be kept in mind when assessing the compressive behavior of these foams. Broken microspheres, usually present in these reinforcements, may be classified by buoyancy in a fluid with higher density than the microspheres [34].

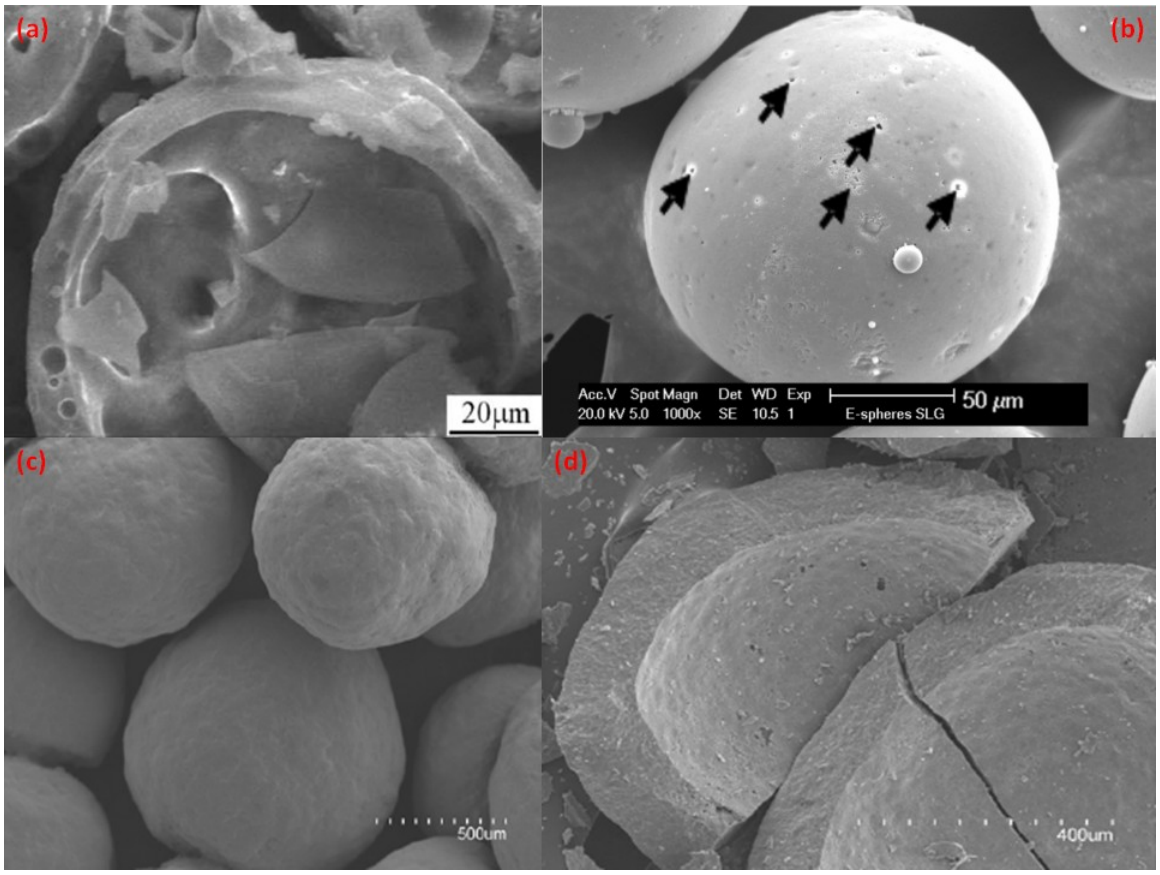

FIG. 1 SEM images of microspheres in (a) broken fly ash, (b) ceramic, (c) SiC, (d) broken SiC [6, 34, 55]

2.3 Mechanical Behavior of Metal Matrix Syntactic Foams

Most of research publications dealing with metal matrix syntactic foams report their compressive mechanical properties because these foams are designed to work mainly under compression, especially those applications related to impact energy absorption. The properties of metal matrix syntactic foams depend on several parameters like particle shell material, shell wall thickness to diameter ratio, matrix alloy, processing parameters, entrapped voids, and heat treatment conditions. In the following sections the general deformation behavior of MMSF will be described in terms of their stress-strain compression curves as well as the effects of matrix strengthening, volume fraction and the t/D ratio on the behavior of these foams.

2.3.1 General Deformation Behavior

The typical shape of a quasi-static compressive stress-strain curve for MMSF is shown in Figure 2 [55] where three clearly differentiated stages of deformation are observed. First, a linear elastic deformation represented by zone I, where the stress increases linearly with strain until reaches a peak stress (σ_0). The second zone (II) starts with a sudden drop in the stress followed by an extended plateau where stress remains essentially constant until a relatively large strain is reached. This is the zone where the energy absorption of MMSF develops, due to a progressive collapse of the hollow spheres. The author differentiates two sub zones, II_1 where disperse collapse of the hollow spheres is produced and II_2 where bands of densification develop due to localized plasticity of the composite. Finally, the zone III represents the densification

stage, which starts with the densification strain (ε_D) and is characterized by a rapid increase in stress for a given differential strain.

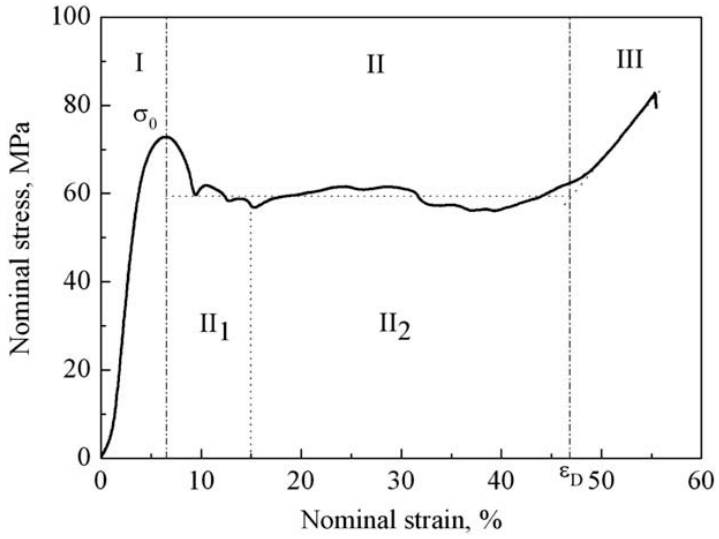

FIG. 2 Compressive stress-strain curve showing different stages of deformation [55]

In this study the densification strain (ε_D) was determined as the intersection of the tangents to the plateau and densification regions, parameter that was used to evaluate the energy absorbed per volume unit (toughness of the MMSF). In reality, the plateau zone is not always as clearly demarked as shown in Figure 2, accordingly a variety of methods have been used in the literature to report the plateau strength of MMSF [8, 25, 31] . In this study the energy absorbed is represented by the area under the compressive stress-strain curve from the peak stress until the densification stress reaches the magnitude of the initial peak stress.

Quasi-static compressive curves exhibit different modes of failure at the peak stress and during densification, as was shown by Balch et al. [4] for commercially pure (cp-Al) and alloyed aluminum matrix syntactic foams. For the case of cp-Al foam Figure 3 shows a

well-rounded peak stress, which means that the matrix yields, i.e. deforms plastically, before the hollow spheres start to fail. The stress drop after the peak stress corresponds to the formation of 45° crush-bands, as indicated by the arrow in the plateau zone. Similar behavior has been also observed for aluminum alloyed syntactic foams with different types of hollow spheres [4, 5, 35, 55].

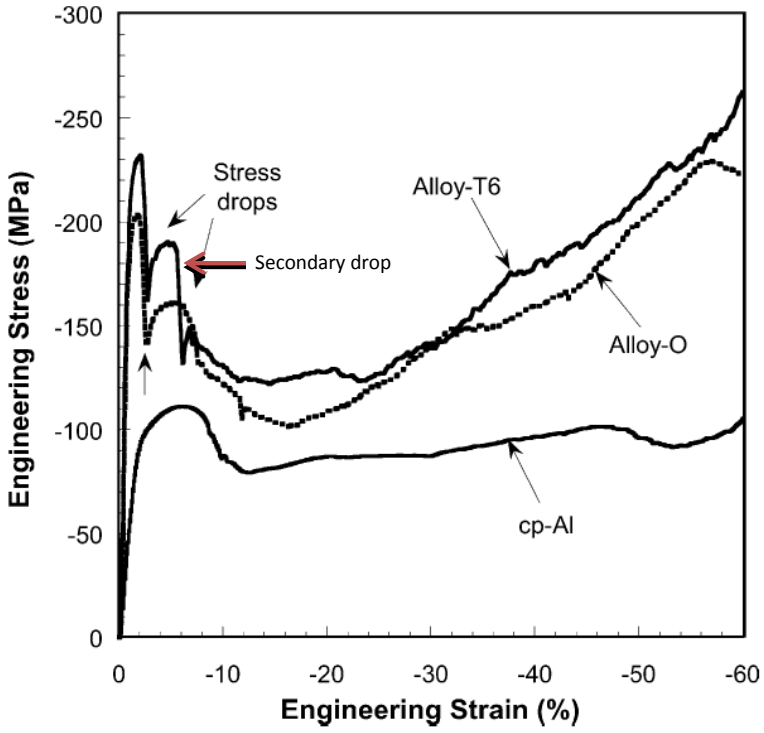

FIG. 3 Quasi-static compressive behavior of cp-Al and alloyed syntactic foams [4]

In the case of the aluminum alloyed foams (O and T6) the hollow spheres failed before the matrix and, a very sharp primary drop and a more rounded secondary drop is observed. This behavior has been explained by the author as the result of two near-45° shear bands of collapsed spheres inside the specimens, probably due to a higher strength and reduced ductility of the matrices (compared with the cp-Al) and to the

presence of strong and brittle ceramic reinforcements in the foams. Similar results have been observed in other alloyed aluminum matrices [4, 6, 8, 15].

A different behavior has been observed in metal matrix syntactic foams containing metallic hollow spheres. Figure 4 shows the stress–strain compressive curves for syntactic foams made up with steel hollow spheres in steel and aluminum matrices, by casting and powder metallurgy, respectively [26].

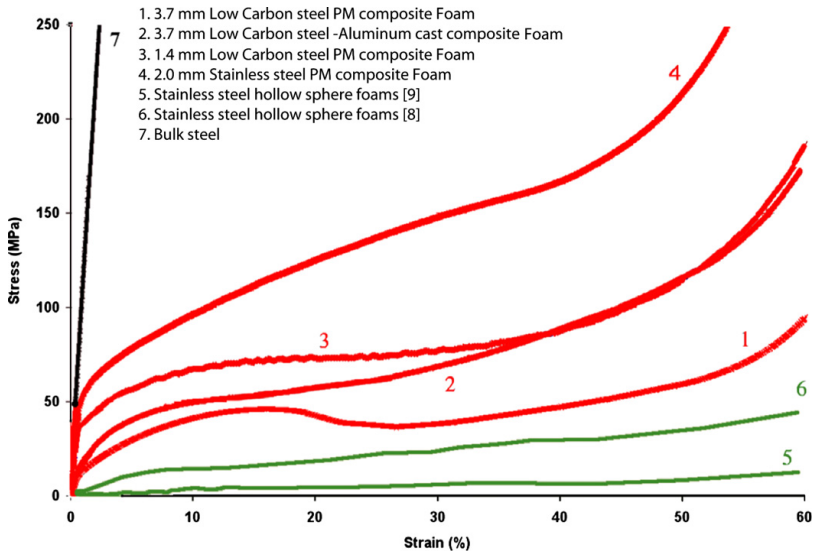

FIG. 4 Strain-stress compressive curves for metallic hollow spheres syntactic foams [26]

In this case the mode of failure under compression is ductile as opposed to brittle ceramic hollow spheres. There is an initial region of elasto-plastic deformation, followed by a non pronounced drop in peak stress and an extended plateau region at a relatively constant stress. This behavior has been also observed in other syntactic foams containing metallic hollow spheres [13, 36].

2.3.2 Matrix Strengthening Effect

As it was shown in the previous section, increasing the peak and plateau stresses of a MMSF improve their energy absorption capabilities. One approach to achieve this aim is by increasing the strength of the matrix through a heat treatment, for those heat treatable alloys. Balch [4] and later on Orbulov [6] have shown the effect of a standardized heat treatment (T6) of aluminum based syntactic foams on their energy absorption capabilities. In both cases the heat treated alloys show higher peaks and energy absorption values that those non treated foams. A similar behavior has been reported by Daoud [37] for the heat treatment of ZnAll22 matrix syntactic foams. According to the author the heat-treated foams exhibit ductile deformation behavior due to their higher plasticity induced by the fine microstructure of the ZnAl22 matrix.

Santa Maria et al. [20] has studied the effect of matrix strength, hollow spheres size and distribution on the compressive properties of syntactic foams made of Al-A206/Al_2O_3. The study covered three different hollow sphere size ranges and was tested in the as cast as well as in the T4 and T7 conditions. The results showed that the peak stress of the syntactic foams follow the yield strength of the heat treated matrices. Also, the peak strength, plateau strength and toughness of the foams increase with increasing the *t/D* ratio of the spheres.

It should be noted that the increase in peak and plateau stresses of syntactic foams, due to their heat treatment, may be not as high as the values found for the heat treated matrix. For aluminum based syntactic foams this behavior has been attributed to a

modification in composition and phases of the original matrix, due to chemical reactions between the melt matrix and the silica of the hollow spheres, leading to the precipitation of silicon inside the matrix and the formation of alumina on the walls of the spheres [6, 27]. This type of chemical interactions between the melt and the hollow spheres can modified drastically the composition of the matrix after the heat treatment.

2.3.3 Volume Fraction Effect

The volume fraction of hollow spheres in syntactic foams will depend on their spatial arrangement inside the metal matrix. Sanders and Gibson [77, 78] studied the mechanics of hollow-sphere foams assuming ordered arrangements of the spheres in space, similar to those found in crystalline systems of metals, i.e. single cubic (SC), body-centered cubic (BCC) and face centered cubic (FCC). Using the packing factors of these crystalline systems, it can be said that the maximum obtainable volume fractions of spheres in syntactic foams (theoretical) would be 0.52, 0.68 and 0.74 for SC, BCC and FCC respectively. After modeling the mechanics of hollow spheres following these arrangements, Sanders and Gibson found that the FCC packing has superior mechanical properties than BCC or SC systems.

The effect of volume fraction on the compressive properties of MMSF has been studied by Tao et al. [17] by infiltrating a mixture of ceramic microballons and Al 6082 alloy powder with a melt of Al 6082 alloy, in this way the volume fraction of the matrix was varied between 37% and 70% of aluminum in the foams. The compressive stress-strain curves showed that as the volume fraction of microballons was decreased a higher peak

stress was higher and the length of the plateau stress was drastically shorter. Regarding the specific energy absorption capability the 50% aluminum foam showed the highest value followed by the 60% and 43% aluminum foams. Similar results were obtained by Daoud et al. [37] who used flyash spheres in a Zn22Al matrix; the same inverse relationship between volume fraction of microballons and peak stress was found, however no values for the specific energy absorption for different volume fractions of flyash was given, therefore no conclusions can be drawn on this parameter.

Other research studies varying the volume fraction of microspheres have been published but using different sizes of spheres [14, 16, 35] with variable results.

2.3.4 Microsphere Wall Thickness/Diameter Ratio (t/D)

The energy absorption capability of MMSF depend on a number of parameters like the material of the hollow sphere, microsphere wall thickness/diameter ratio, microspheres size range, matrix alloy, processing parameters, unintended porosities and heat treatment conditions. In this section the microsphere wall thickness/diameter ratio (t/D) effect will be reviewed.

This effect has been studied in detail by Kiser et al [9], where alumina microspheres of three different (t/D) ratios were infiltrated by A201 and A360 aluminum alloys. The stress-strain compressive curves shown that the peak stress increases as the wall thickness/diameter increases, by a factor of up to 3. This behavior was observed in the three matrices (A201-O, A201-T6 and A360-O). Santa Maria et al. [19] presented a graph with a review of published quasi-static compressive properties of syntactic foams with

approximately 60% of microspheres. The graph shows the same trend as Kiser's work, there is direct relationship between peak stress and (t/D) ratio of microspheres.

2.4 Applications of Metal Matrix Syntactic Foams

During the last decade metallic foams, either with open or close cells has been used in industry, basically in transportation, defense and aerospace applications. MMSFs exhibit many desired combinations of physical and mechanical properties including high specific stiffness, high specific energy absorption, and low thermal conductivity that make them ideal for replacing metallic foams in many of their current applications.

The growing importance of these metal matrix syntactic foams has been stressed by G. M. Gladysz et al. [52] in a graph that shows the steep increase of research publications on syntactic and composite foams since 2003, possible driven by the industry trend for increasing functionality; whether for reduced weight for fuel saving or for optimum functionality of biocompatible structures.

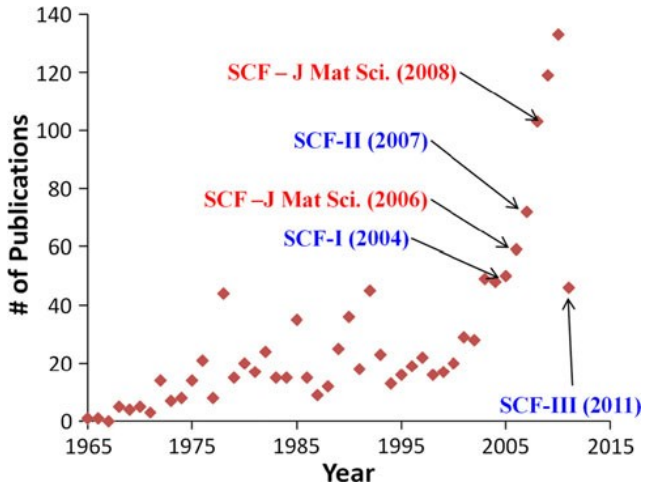

FIG. 5 Increase in syntactic and composite foams publications (1965-May 2011) [52]

2.4.1 Ground transportation

This segment has the largest share of the world market for metal matrix composites, and this is expected to grow with the demands for low fuel consumption and safety in the automotive transportation industry [53]. One approach to satisfy both demands is through the use of metallic foams and metal matrix syntactic foams. An aluminum-fly ash cenosphere composite is being promoted by an Australian company under the trademark ULTALITE® [54]. This MMC is made of A356 aluminum alloy with Fly-ash cenospheres, in the range of 10% to 50% by weight. The producer claims this composite could be used for manufacturing several automotive components like brake drums, brake discs, engine blocks, cylinder heads, pistons, con rods, oil pumps, and transmission components.

MMSFs are excellent energy absorbers due to their deformation at a nearly constant stress level over a wide range of strain making them ideal for crash energy absorption zones in ground transportation [55]. Metallic foams and MMSFs have a low rebound performance in dynamic crash situations, e.g. aluminum foams with less than 3% in comparison with 15% of polyurethane foams [56]. Also, it should be noted that MMSFs have a much better performance as energy absorbers than metallic foams [57]. Some of the potential applications of foam-filled structures include crash boxes for head-on impacts, and under-ride protection for semi-trailer trucks.

MMSF's may be also used to improve crash energy absorption in high speed rail equipment as shown by a study by Kremer et al. to identify, investigate and

demonstrate specific applications for aluminum foam in high speed rail equipment [58]. The application areas explored include: lightweight aluminum foam sandwich panels for flooring, partitions and electrical panel doors, primary impact energy absorption in sliding sills or crushable zones at the end of passenger cars, secondary head impact energy absorption to reduce head injury, and energy absorbing sliding seat rail to reduce injury to passengers on impact with seat backings.

2.4.2 Aerospace

A promising application of MMSF that has been explored by turbines manufactures is the construction of aerofoils. Rolls-Royce Plc has registered a patent in the USPTO for a method of manufacturing an aerofoil for a gas turbine engine, either for the rotor blade or the stator vane [59]. The aerofoil is made of a laminate with two metal sheets and a core of syntactic foam and, according to the patent claims the syntactic foam can be made of aluminum, titanium, nickel, magnesium, or steel alloys. Powdermet Inc. has proposed aluminum and titanium syntactic foams as a replacement for energy absorbing casements for the interior of the fan case in turbine engines as a light weight alternative to hard wall fan casings and a more compact alternative to soft walled fan casings [60].

2.4.3 Defense

The current needs of the armed forces include quicker deployment of vehicles, personnel, and armaments as well as better protection of personnel in combat. A common approach for achieving ballistic impact resistance and energy absorption

performance is the design of functionally graded armor composites (FGACs) [61]. These are generally laminated materials consisting of a front-facing layer whose purpose is to blunt and abrade the incoming projectile; meanwhile a second layer supports the facing material during this initial impact and then deforms and absorbs energy. Typically, the front-facing material is a ceramic, usually Al_2O_3, while the backing layers are typically light metals such as aluminum, but recent developments include fiber composites that provide a better combination of energy absorption and reduced weight [62]. While metal foams have been shown to offer little in the way of ballistic protection [63], when implemented as intermediate layers between the MMC or ceramic face-plates they may act to reduce stress-wave transfer and to allow the projectile to be slowed by crushing the foam before the backing material is deformed [64].

The US Navy has extensively researched and developed lightweight and high performance composite materials as alternatives to monolithic metals to address their need to enhance the operational performance of naval vessels, i.e. increased range, stealth, stability and payload. Rawal and Lanning report the development of a ceramic microballoon reinforced Ti/$((Al_20_3)_{mb}$/Al)//Ti composite panel for advanced submarine applications [65]. The physical structure of the composite was a laminate made of two Titanium sheets as the outer faces and the syntactic metal foam (Al_2O_3 microballons in an aluminum matrix) sandwiched between them. This combination offered low-density, good compressive strength, high damping, and impact resistance compared to the conventional HY-80 steel used for submarine hull and joint ring, and platform structures. Despite the promise of these new materials, most of the completely developed

applications of lightweight composites are found only on relatively small naval ships or in non-structural components on large ships and submarines [66].

2.4.4 Biomedical

Titanium alloys have been widely used in orthopedic implants due to their good biocompatibility, high strength to weight ratio relative low elastic modulus, high fatigue strength, and excellent corrosion resistance. However, a disadvantage with the use of these materials is that the implant often will become loose (disruption of the implant/bone or cement interface) due to a stress-shielding effect between the higher stiffness Titanium alloy (aprox. 120 GPa) and the bone (aprox. 18.6 GPa) [67-68]. This phenomenon leads to bone loss and weakening of the bone. One strategy to reduce this effect is to use implant materials that mimic the structure and properties of human bone, where the distribution of load in the bone/implant is not altered by the presence of the implant. Since bone is an anisotropic material and varies in its mechanical properties throughout the body, composite materials are an ideal choice where tailored and functionally gradient properties may be achieved. Preliminary studies on the mechanical and biological properties of a Ti-ceramic microsphere (diameter: 150 µm, composition: ~60%SiO_2, ~40%Al_2O_3, 0.4-0.5% Fe_2O_3) syntactic foam, manufactured by powder metallurgy have been reported [69]. The data reported in this study suggests that titanium alloy matrix syntactic foams have potential for orthopedic implant materials and warrant further investigation.

2.4.5 Building applications

Metal matrix syntactic foams offer many significant advantages for structural applications due to their high specific stiffness, impact energy and sound and energy absorption capabilities. Civil engineering and structural applications that have been proposed include lightweight framing and structures, thermal insulation, and protective structures, however as processing costs remain high such applications will likely be limited to very specific niches where the performance outweighs the cost. An interesting study by Salimon et al. [70] shows, based on a materials selection methodology, potential applications of steel and titanium foams, which may be a close analog for the properties of typical aluminum alloy MMSFs. Potential applications predicted for metallic foams in building applications are [70, 71]: flooring, decoration, roof and ceiling, lightweight fire doors and hatches, and elevators.

2.4.6 Electronic Packaging

Dou et al. [72] found that Al-2024-fly ash syntactic foam was superior to Al-2024 for electromagnetic shielding applications. In the frequency range of 1–600 MHz the EM shielding property of 2024Al alloy was in the range −36 to −46 dB while that of the composites was in the range of −40 to −102 dB. With careful selection of the matrix and hollow microspheres material new classes of lightweight high performance electronic packaging materials may be developed.

2.5 Summary of Literature on MMSF

Summarizing, it can be said that several methods are available for the synthesis of metal matrix syntactic foams. Pressure infiltration the most widely used method for synthesizing foams with metallic matrices of low melting point, while powder metallurgy seems to be the preferred method for syntactic foams with high melting point matrices.

The processing of MMSFs present some technological problems that should be addressed to avoid undesirable mechanical properties derived from chemical reactions between the matrix and the reinforcement, unintended porosity and the quality of the hollow spheres.

The compressive mechanical properties of metal matrix syntactic foams depend on several parameters like particle shell material, shell wall thickness to diameter ratio, matrix alloy, processing parameters, entrapped voids, and heat treatment conditions.

MMSFs present a clear advantage over metallic foams due to their light-weight, high specific strength and specific stiffness and high energy absorption properties. These advantages make them excellent candidates for applications in ground transportation, aerospace and defense. However, the lack of design data, lack of high quality hollow reinforcements, high cost of their manufacture and lack of multiple suppliers affect adversely the development and manufacturing of MMSF components.

3. Experimental Procedure

Syntactic foams composed of aluminum alloy Al-A206 and magnesium alloy Mg-AZ91 reinforced with approximately 50 v% hollow SiC spheres (1 mm nominal diameter, 70 µm wall thickness, and 0.7 g/cm^3 bulk density from Deep Springs Technology) were synthesized via a sub-atmospheric pressure infiltration technique. The nominal compositions of the alloys are presented in Table I.

The infiltration method used to synthesize the MMSFs for this study is described in detail elsewhere [38] and is summarized below. A 12.7 mm x 12.7 mm steel tube with one end welded shut was tap-packed with hollow spheres to a height of 35–50 mm. A 2 mm thick layer of zirconia felt was placed on top of the tap packed spheres, and finally an ingot of either Al-A206 or Mg-AZ91 alloys was placed inside the tube on top of the zirconia felt to complete the assembly. The zirconia felt is used as a reaction barrier between the aluminum or magnesium alloy melt and the spheres prior to infiltration and served as a filter to remove the oxide layer from the liquid melt, as shown in Figure 6. The assembly was then heated in a quartz chamber under vacuum to 750^{o}C in the case of Al-A206 and 650^{o}C for Mg-AZ91, and held for 60 minutes at which time the alloy had fully melted and created a uniform seal on the inner perimeter of the steel tube. Argon gas was then rapidly introduced into the heated quartz chamber until a sub-atmospheric pressure of 0.5 bar was reached, thereby forcing the molten alloy into the evacuated spaces between the hollow spheres.

TABLE I. Nominal composition of matrix and reinforcements.

Material	Component	Nominal Content (wt %)
Al-A206	Al	93.3-95.3
	Cu	4.25-5.0
	Fe	0.1
	Mg	0.15-0.35
	Mn	0.2-0.5
	Ni	0.05
	Si	0.05
	Sn	0.05
Mg-AZ91	Mg	88-91
	Al	8.3-9.7
	Mn	0.13 min
	Zn	0.35-1.0
	Si	0.50 max
	Cu	0.1 max
	Ni	0.03 max

The quartz chamber containing the sample was kept in the tube furnace at a sub-atmospheric pressure of 0.5 bar for 10 minutes. The sample was then removed and quenched in room temperature water.

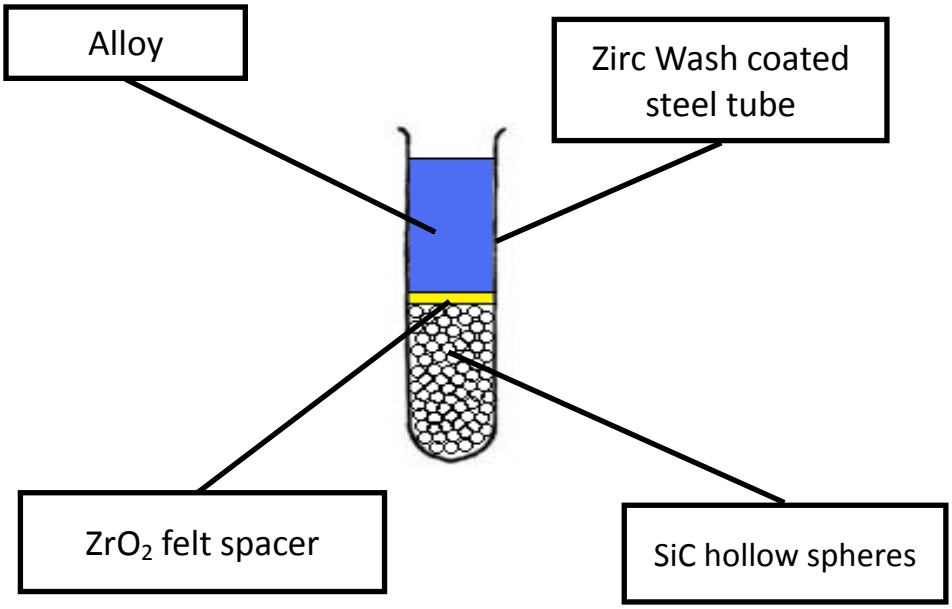

FIG. 6 Syntactic Foam Assembly

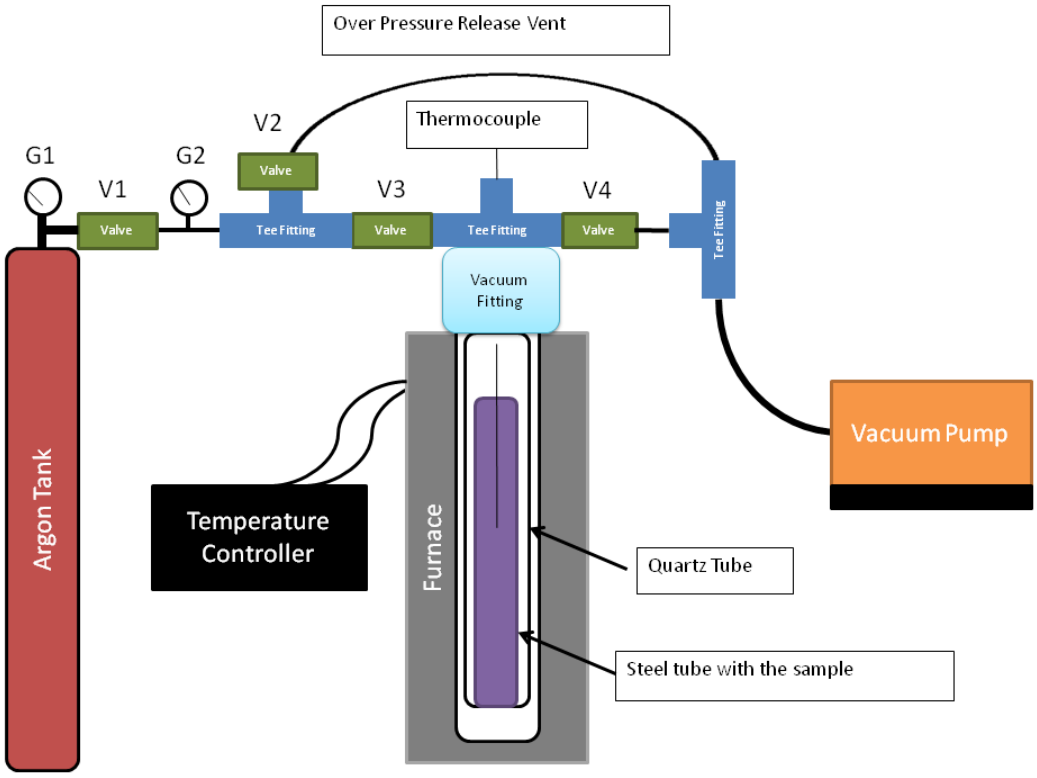

FIG. 7 Schematic of Low Pressure Infiltrator

The infiltration pressure was determined after some trials, in order to get a pressure where most of the spheres were surrounded by the matrix (well infiltrated) with the least amount of spheres filled by metal. The assembly used in the study is shown in Figure 7. Specimens of the unreinforced alloys were cast using the same procedure described above for comparison with the syntactic foams. Following casting, the specimens were de-molded to give final dimensions of 10.4 mm x 10.4 mm x 35-50 mm. Portions of the Al-A206 alloy specimens were heat treated to the T4 and T7 conditions respectively.

Those samples that were heat treated were first solutionized at 490-500 ^{o}C for 2 hours followed by 525-530 ^{o}C for 14-20 hours. Then they were aged at 21 ^{o}C for 120 hours for

the T4 condition, and 4 hours at 200 ^{o}C for the T7 condition [39]. The Mg-AZ91 alloy specimens were tested in the as-cast condition.

Optical microstructures were obtained using a Nikon Eclipse TS100 microscope. A Topcon SM300 scanning electron microscope equipped with EDS was used to identify the composition of phases. The density of the composites was measured using a Metler Toledo AT261 Delta Range Microbalance equipped with a density measurement apparatus (Archimedes method). The specimens were first lightly coated with vacuum grease to prevent infiltration of surface pores during the density measurement.

Quasi-static compression testing was performed in accordance with ASTM C365-11 on specimens sectioned into cubes having dimensions of 10.4 mm x 10.4 mm x 10.4 mm. Testing was carried out using a SATEC Model 50Ud Universal Testing Machine at constant crosshead speed with an initial strain rate of 10^{-3} s^{-1} and a self-leveling platen. Strains were calculated from the crosshead displacement, and were corrected for deflection of the load frame. The quasi-static compression curves typically exhibited an initial peak followed by a lower plateau stress and later densification. Compression was stopped when the densification stress slightly exceeded the magnitude of the initial peak stress. . The toughness of the MMSFs was determined by calculating the area under the quasi-static compressive stress strain curve up to the densification strain and has units corresponding to the energy per unit volume of the material (J/cm^3). A variety of methods have been used to report the plateau strength [13, 34, 36, 55]. The plateau strength reported in this work is the average of all the measured stress data points

between the strain corresponding to the initial peak stress and the densification strain (the strain following the initial peak strength at which the stress reaches the magnitude of the initial peak stress) [34].

The high strain rate compressive properties of MMSFs are of technological interest due to their high energy absorption properties and possible application to blast mitigating structures. Aluminum alloys and aluminum alloy composites do not typically exhibit strain rate dependence [73], however magnesium alloys are known in some cases to show a higher peak strength under high strain rate conditions [74, 75]. Therefore, the Mg-AZ91/SiC syntactic foams synthesized in this work were tested under high strain rate conditions using a Split-Hopkinson pressure bar test apparatus. Details of the test apparatus and methods are discussed at length elsewhere [76] and are summarized as follows. The cube compression specimens described previously were nested between Inconel incident and transmitter bars having Young's modulus, density and sound wave velocity of 195 GPa, 8190 kg/m^3 and 4802 m/s respectively. Once a test is performed by launching a striker bar into the incident bar which crushes the specimen, data from strain gages mounted at the centers of the incident and transmitter bar is obtained and used to calculate the stress, strain, and strain rate. In this work strain rates between 537 and 726 s^{-1} were achieved.

4. Results and Discussion

4.1 Microstructure

The properties of metal matrix syntactic foams have been shown to depend greatly on both the t/D ratio of the spheres and the properties of the matrix. Features of the matrix that will have an effect on the foam's properties include:

- the presence of defects such as unintended porosity or inclusions,
- the final matrix composition (especially in cases where the matrix reacts with the reinforcement),
- fineness of the microstructure
- the distribution of phases that form as a result of the solidification sequence in the case of as-cast composites or as a result of the heat treatments.

Figures 8 and 10 show microstructures of metal matrices Al-A206 and AZ91D, side by side with their respective syntactic foams, for the different conditions used in the study. Regarding Al-A206 base alloy and Al-A206/SiC syntactic foams, Figures 8a and 8b show microstructures for the as-cast condition, Figures 8c and 8c microstructures for T4 tempering condition, and Figures 10a and 10b correspond for T7 tempering condition. Figures 10c and 10d show microstructures of AZ91D base alloy and AZ91D/SiC syntactic foam for the as-cast condition.

The as cast microstructure of Al-A206 consists of a dendritic structure of α-phase, whose interdendritic regions are generally made up of Al, Al_2Cu, $Al_2Mn_3Cu_2$ and Al_7FeCu_2 phases as a result of the eutectic reaction [40, 41]. Figure 9 show SEM

micrographs of the base alloys Al-A2036 and Mg-AZ91, and was used to confirm the presence of phases found; the composition of these phases was determined by EDS and the results are presented in Table II. As shown in Figures 8c, 8d, 10a and 10b, the interdendritic phases present in the as-cast alloy were only partially dissolved by the solutionizing heat treatment employed which may be due to dissolution of Fe from the mold during processing.

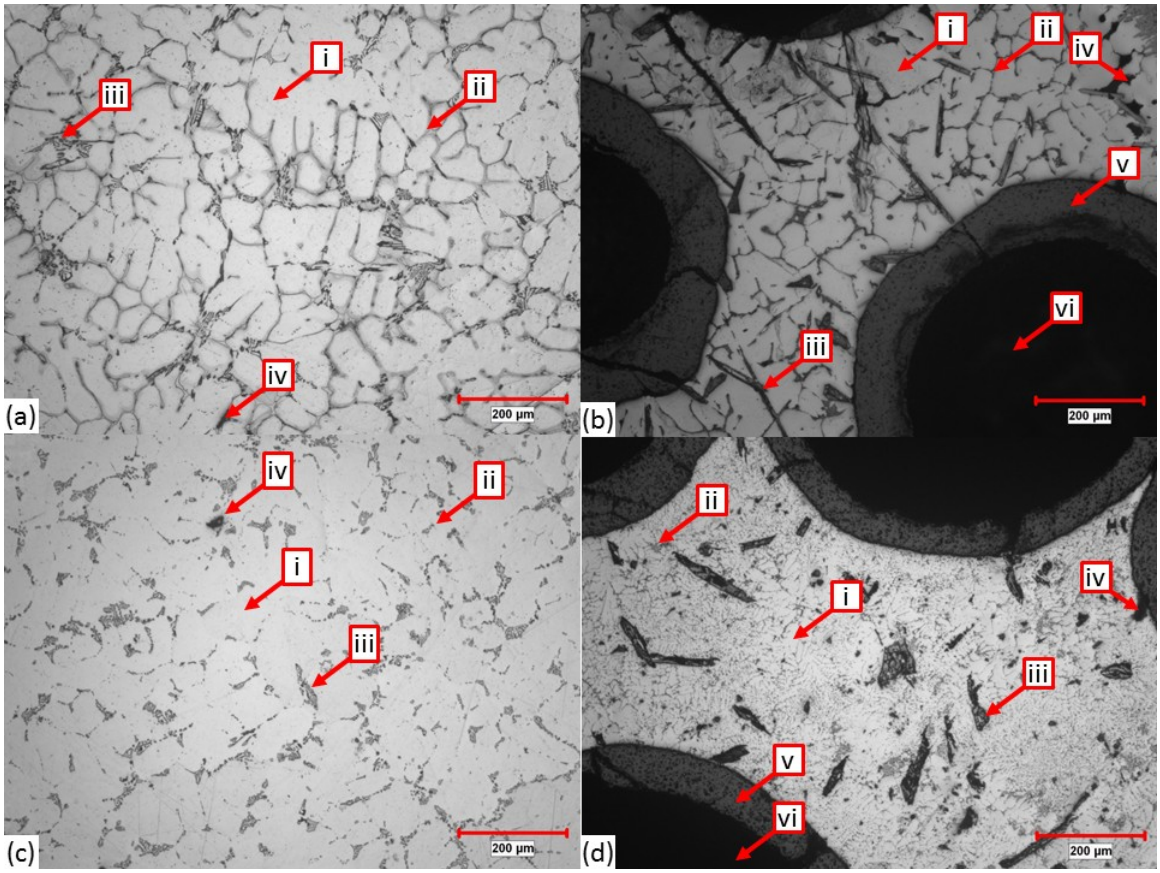

FIG. 8. Representative microstructures of Al-A206 without reinforcement in: a) as-cast and c) T4 conditions; and their respective Al-A206/SiC syntactic foams synthesized in: b) as cast and d) T4 conditions. Unique phases and microstructural features visible in these micrographs are labeled as follows: i. α-Al, ii. bright intermetallic (typical of A206), iii. dark intermetallic (likely present due to Fe dissolution), iv. porosity, v. SiC hollow sphere wall, vi. hollow pore within SiC sphere.

The microstructure of the Mg-AZ91 magnesium alloy cast under the same conditions as corresponding syntactic foam is shown in Figure 10c. Under these casting conditions, the microstructure is clearly dendritic and is composed of α-Mg dendrites surrounded by both course and lamellar intermetallics (typically $Mg_{17}Al_{12}$, the measured compositions are shown in Table II) [42, 43]. Interdendritic porosity was also observed.

Figure 11 show SEM micrographs of syntactic synthesized in this study, was used to confirm the presence of phases found. Table III presents the results of EDS analysis of the various phases labeled in Figure 11. The hollow spheres appear to be uniformly distributed, and fully encapsulated by the metal matrix with little to no visible porosity in the matrix between the hollow spheres. The Al-A206 as-cast samples show a network of intermetallics throughout the matrix similar to that found in the base alloy without reinforcement.

Following the T4 and T7 heat treatments, the intermetallic network present in the as-cast specimens was partially dissolved and precipitated during the aging treatments. Coarse phases containing Fe and Si were also observed to be dispersed in the Aluminum alloy specimens. The formation of these intermetallics may be as a result of the presence of excess Si in the matrix due to the partial reaction of the SiC spheres to form aluminum carbides [44], as well as partial dissolution of the steel tube that was used as a crucible. Some cracking of the spheres is also observed in these micrographs, which likely occurred during or after solidification due to CTE mismatch as there is little to no infiltration of the spheres. The microstructure of the Mg-AZ91/SiC syntactic foam shows refinement in comparison to the matrix alloy cast under similar conditions, which is

likely due to the restricted solidification of the liquid in spaces between spheres. EDS of the Mg-AZ91/SiC syntactic foams showed the presence of intermetallics containing small amounts of Si that may be present due to the reaction of the SiC hollow spheres with the alloy matrix [45]. The presence of silicon in the alloy may result in the formation of a coarse "Chinese script" Mg_2Si intermetallic phase that is detrimental to the mechanical properties of Mg alloys [42], however this intermetallic phase was not observed in the syntactic foams synthesized in this study.

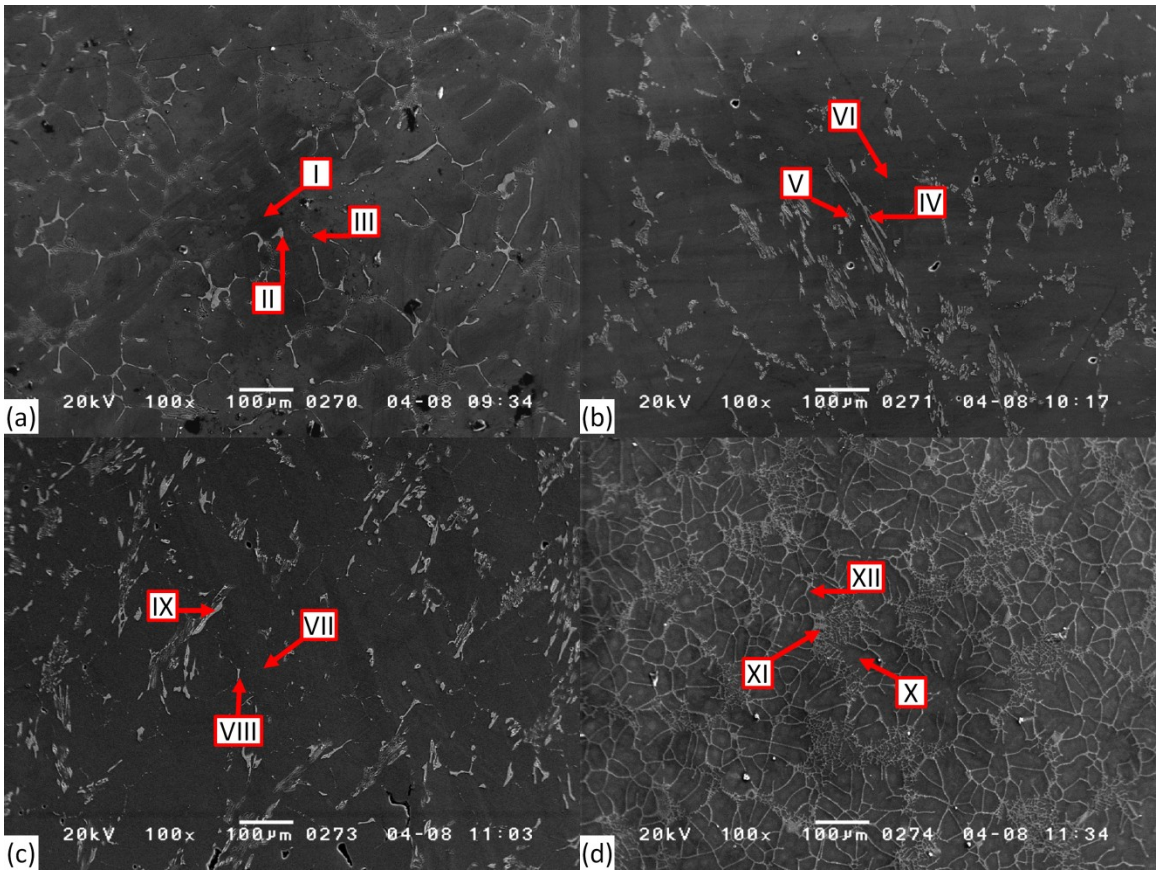

FIG.9. SEM micrographs of Al-A206 without reinforcement in a) as cast, b) T4, c) T7 conditions and Mg-AZ91 in the d) as-cast condition. EDS was used to identify composition of the labeled phases (I-XII) and the results are tabulated in Table II.

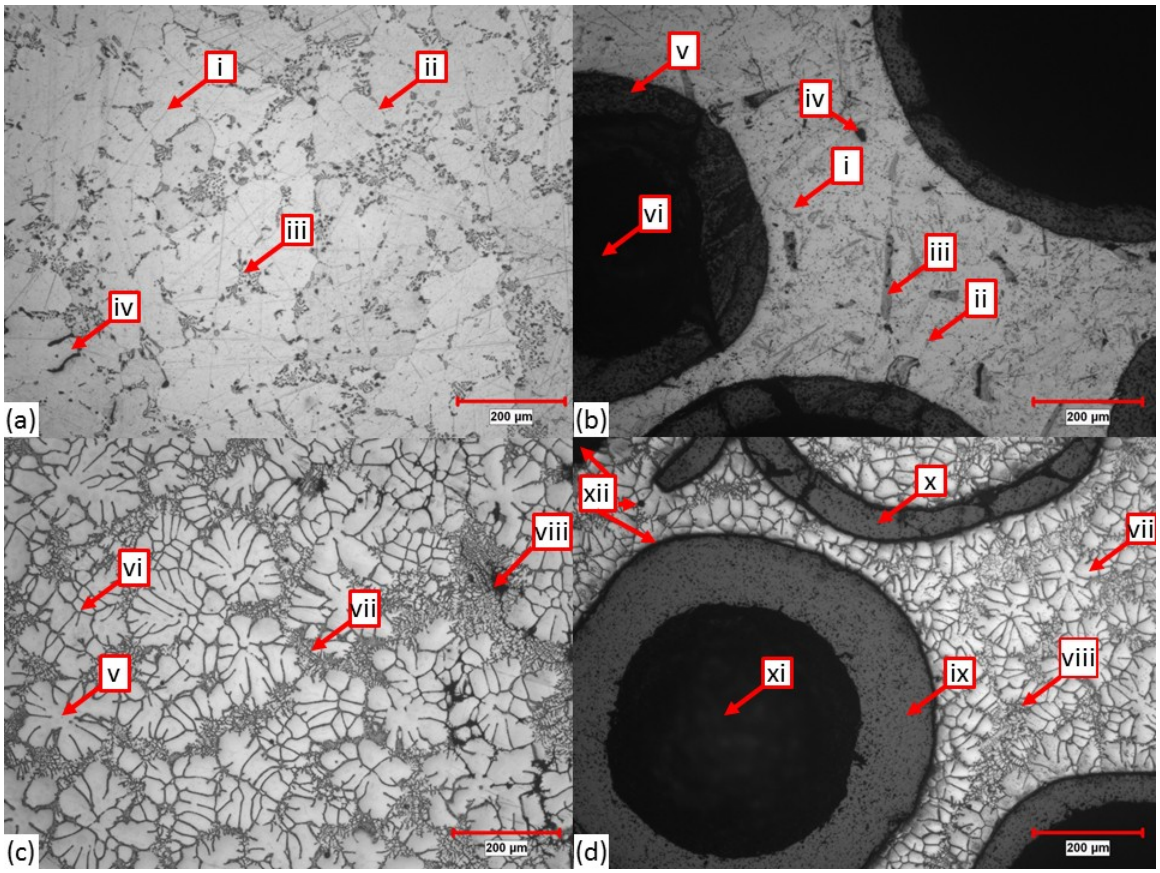

FIG. 10. Representative microstructures of Al-A206 in a) T7 condition and Mg-AZ91 in c) as cast condition, both without reinforcement. Their respective Al-A206/SiC and Mg-AZ91/SiC syntactic foams are shown in b) T7 condition and d) as cast condition. Unique phases and microstructural features visible in these micrographs are labeled as follows: {in parts a - b} i. α-Al, ii. bright intermetallic (typical of A206), iii. dark intermetallic (likely present due to Fe dissolution), iv. porosity, v. SiC hollow sphere wall, vi. hollow cavity within SiC sphere ; {in part c} v. α-Mg, vi. coarse intermetallic, vii. lamellar intermetallic, viii. porosity; {in part d} vii. α-Mg, viii. intermetallic, ix. SiC hollow sphere wall, x. cracked and filled SiC sphere, xi. hollow pore within SiC sphere, xii. porosity.

TABLE II. Compositions of the various phases formed in Al-A206 and Mg-AZ91 base alloys (processed under the same conditions as the syntactic foams produced in this study) evaluated by SEM/EDS. Roman numerals in the first column refer to the annotations shown in Figure 10.

Area	Matrix	Al (at%)	Fe (at%)	Mg (at%)	Cu (at%)	Zn (at%)	Mn (at%)	O (at%)
I	A206/ As-cast	98.01	0	1.81	0.17	0	0	0
II	A206/ As-cast	72.23	0	2.08	25.69	0	0	0
III	A206/ As-cast	88.33	4.96	2.15	4.07	0	0.49	0
IV	A206/ T4	77.40	5.41	1.67	13.75	0	0	1.78
V	A206/ T4	74.21	7.43	0.77	15.97	0	0.76	0.86
VI	A206/ T4	97.34	0	1.35	1.31	0	0	0
VII	A206/ T7	98.00	0	1.90	0.10	0	0	0
VIII	A206/ T7	80.46	6.64	0.10	12.80	0	0	0
IX	A206/ T7	81.80	5.38	1.94	10.88	0	0	0
X	AZ91/ As-cast	1.90	0	98.09	0	0.01	0	0
XI	AZ91/ As-cast	29.11	0	69.36	0	0.37	0	1.15
XII	AZ91/ As-cast	22.49	0	74.63	0	1.02	0	1.86

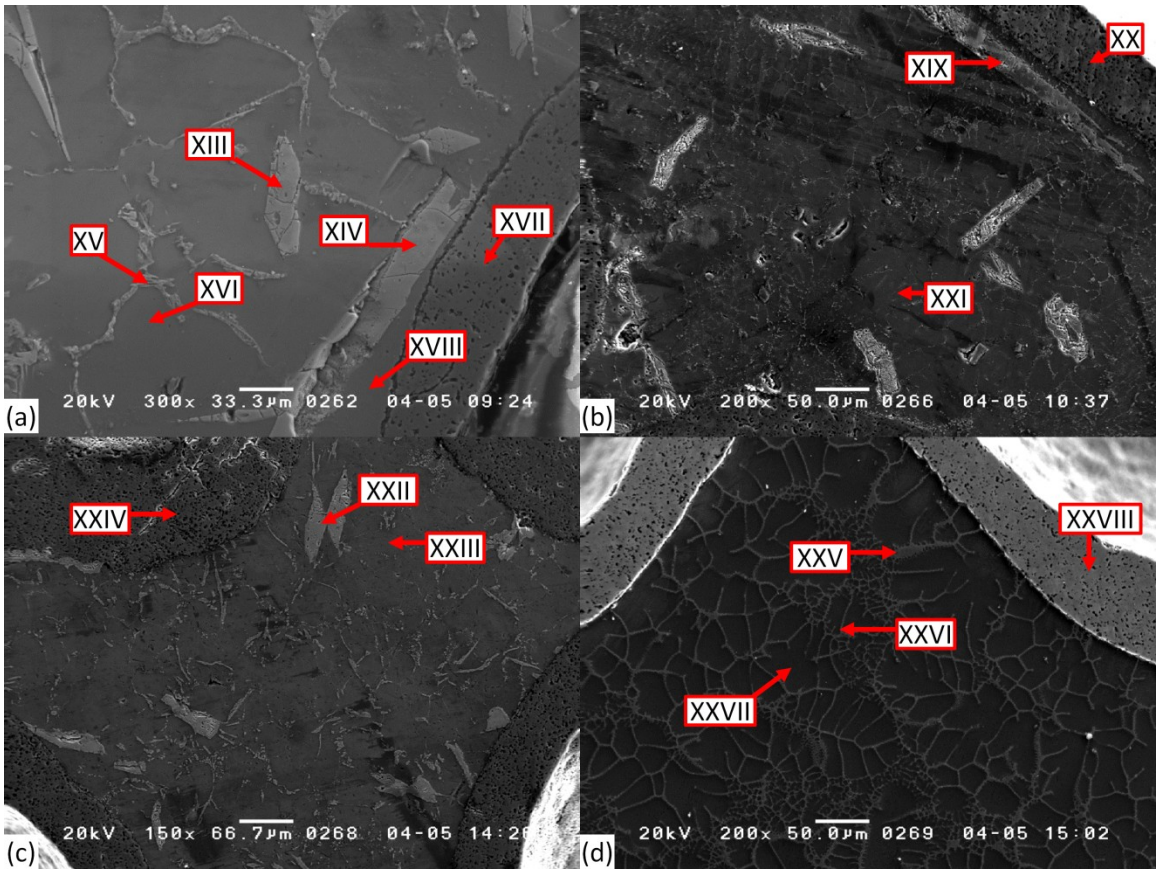

FIG. 11. SEM micrographs of the Al-A206/SiC (a-c) and Mg-AZ91/SiC (d) syntactic foams synthesized in this study. The micrographs for the Al-A206/SiC foams are shown in the a) as-cast, b) T4, and c) T7 conditions respectively. EDS was used to identify composition of the labeled phases (XIII-XXVIII) and the results are tabulated in Table III.

4.2 Quasi-static Compression Properties

Table IV reports the values of peak strength, plateau strength, densification strain and energy absorption for the syntactic foams synthesized in this study. Representative quasi-static engineering stress-strain curves are shown in Fig. 12. From this data, Fig. 13 suggests that the peak stress in this work is influenced by yield strength, as peak stress increases from as cast to T4 to T7, which is similar to the trend in yield stress in the case of the unreinforced alloy.

TABLE III. Compositions of the various phases formed in Al-A206/SiC and Mg-AZ91/SiC syntactic foams evaluated by SEM/EDS. Roman numerals in the first column refer to the annotations shown in Figure 11.

Area	Matrix/ Condition	Al (at%)	Si (at%)	Fe (at%)	Mg (at%)	Cu (at%)	Zn (at%)	Mn (at%)	C (at%)	O (at%)
XIII	A206/ As-cast	78.52	0.89	16.75	2.52	0.59	0	0.73	0	0
XIV	A206/ As-cast	74.60	1.04	20.62	2.19	0	0	0.94	0	0
XV	A206/ As-cast	72.66	2.77	3.80	1.76	13.58	0	0	0	5.43
XVI	A206/ As-cast	97.61	0	0	1.80	0.59	0	0	0	0
XVII	A206/ As-cast	1.95	94.37	0	0	0	0	0	3.67	0
XVIII	A206/ As-cast	97.27	0	0	1.99	0.74	0	0	0	0
XIX	A206/ T4	76.14	0.53	20.59	1.27	0.60	0	0.87	0	0
XX	A206/ T4	1.76	96.65	0	0	0	0	0	1.59	0
XXI	A206/ T4	97.25	0	0	1.95	0.81	0	0	0	0
XXII	A206/ T7	76.83	0.20	19.03	1.32	0.97	0	1.66	0	0
XXIII	A206/ T7	97.84	0	0	1.82	0.34	0	0	0	0
XXIV	A206/ T7	0.71	96.91	0	0	0	0	0	2.38	0
XXV	AZ91/ As-cast	18.98	0.18	0	76.75	0	0.89	0	0	3.19
XXVI	AZ91/ As-cast	21.87	0.47	0	74.82	0	1.06	0	0	1.77
XXVII	AZ91/ As-cast	2.01	0.25	0	95.86	0	0.15	0	0	1.72
XXVIII	AZ91/ As-cast	1.58	92.48	0	0	0	0	0	5.94	0

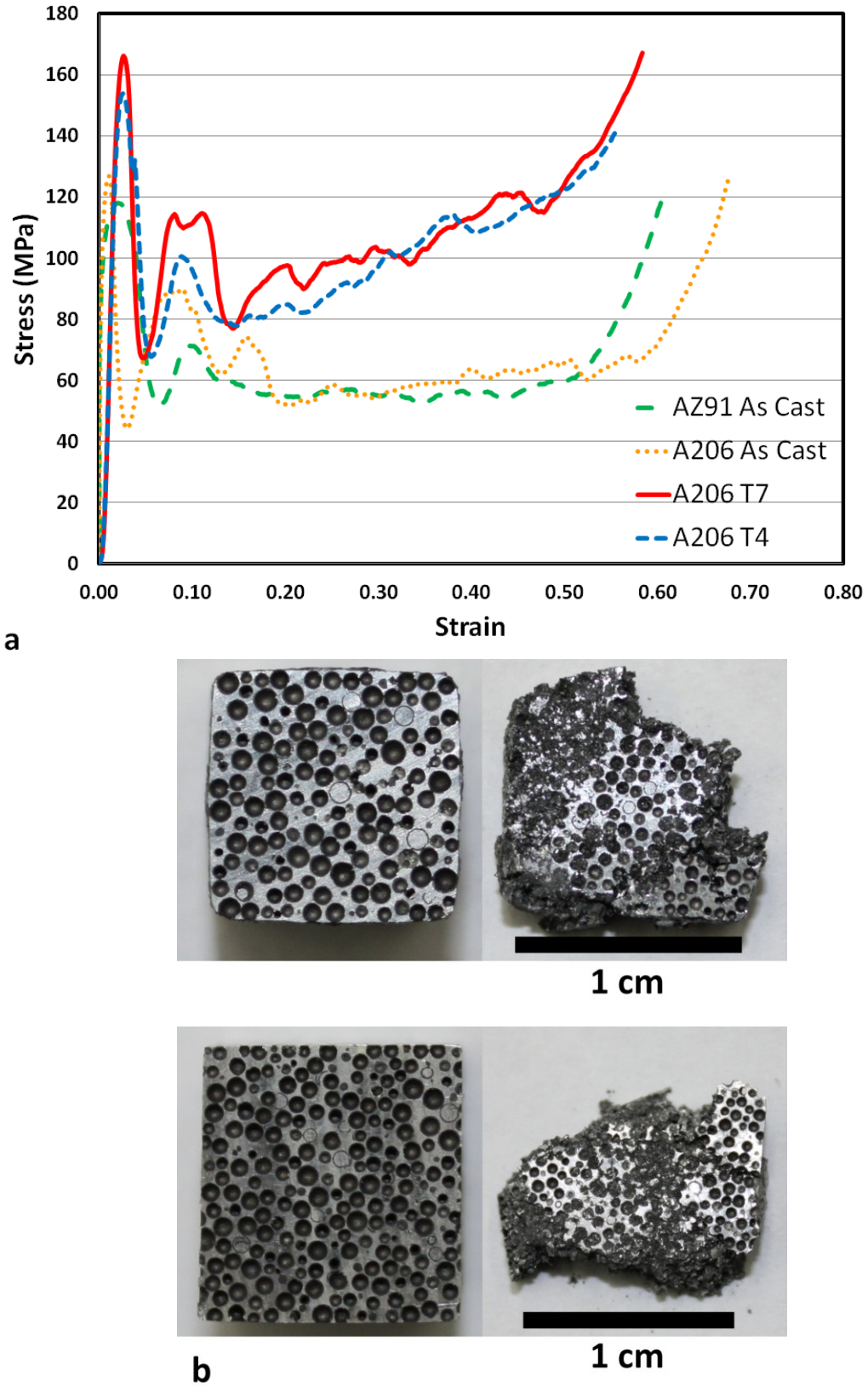

FIG. 12. a) Typical compressive stress-strain curves for Al-A206/SiC and Mg-AZ91/SiC syntactic foams. b) Fractured specimens tested in compression under quasistatic strain

rates shown in the pre-test (Left side) and post-test (Right side) conditions. The top two specimens are Al-A206/SiC syntactic foams and the bottom two are Mg-AZ91/SiC syntactic foams.

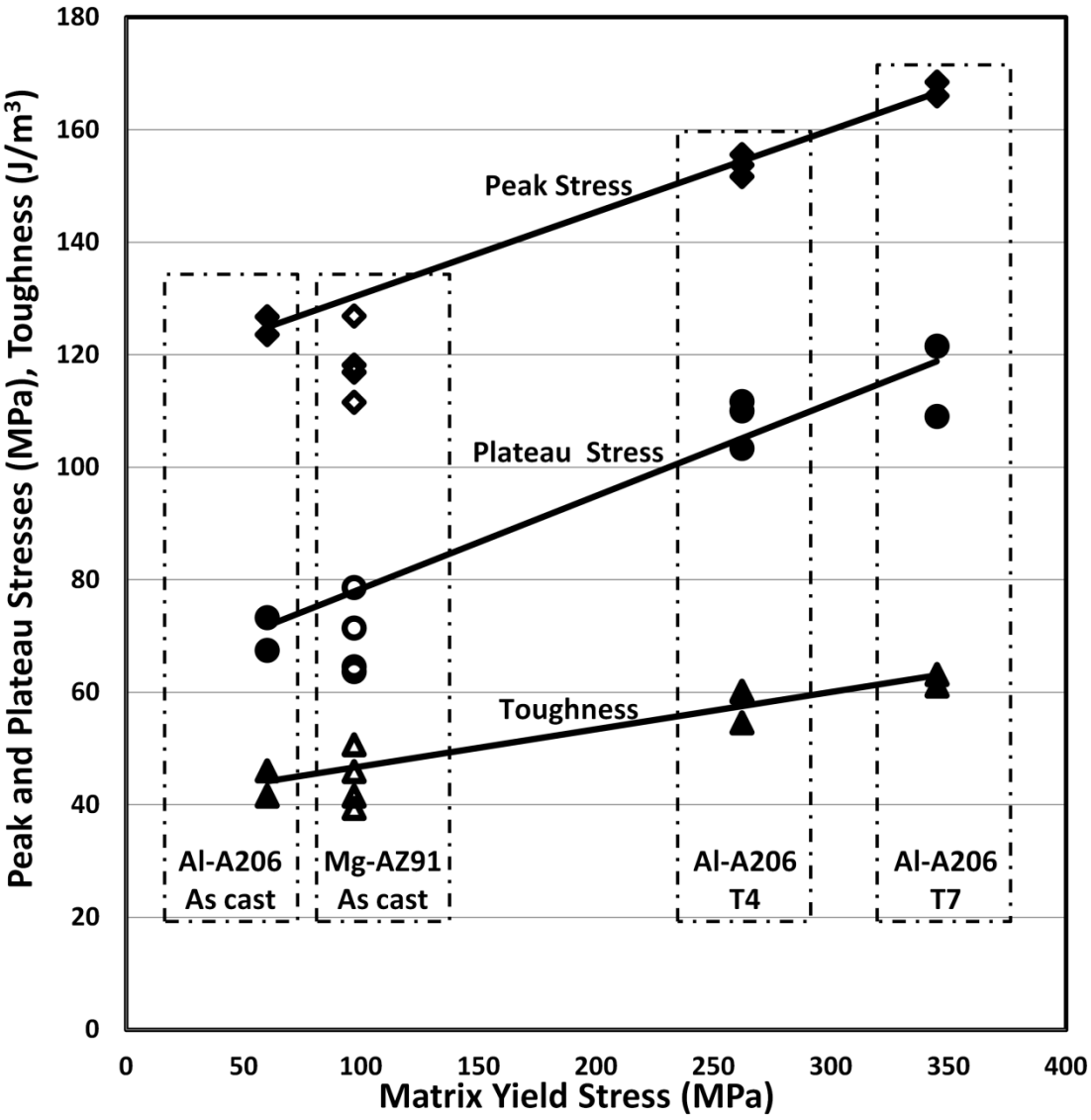

FIG. 13. Average peak strength, plateau strength and toughness vs. yield strength of the base alloy.

TABLE IV. Summary of quasi-static compression data for Al-A206/SiC and Mg-AZ91/SiC syntactic foams

Matrix	Condition	Matrix Yield Stress (MPa)	Peak Stress (MPa)	Plateau Stress (MPa)	Toughness (J/cm^3)	Densification Strain (%)	Density (g/cm^3)
Aluminum Al-A206	As Cast	60*	126.8	67.5	46.1	68%	1.87
			123.6	73.3	41.6	56%	1.89
	T4	262[50]	155.6	111.7	60.1	55%	1.91
			151.7	110.1	60.2	55%	1.93
			153.8	103.4	54.6	53%	1.93
	T7	345[50]	166.1	109.1	63.2	58%	1.93
			168.5	121.5	61.1	51%	1.95
Magnesium Mg-AZ91	As Cast	150[51]	126.9	78.6	50.7	64%	1.20
			116.9	71.4	45.9	63%	1.22
			111.6	64.6	41.5	63%	1.21
			118.2	63.7	39.4	60%	1.21

(*): Estimated

4.3 High Strain Rate Compression Properties

Figure 14a shows the stress strain curves for the Mg-AZ91/SiC under the various strain rates tested. It should be noted that in Split Hopkinson Pressure Bar testing, only the time equal to the stress pulse width is available for deforming the specimen, and thus if the specimen does not reach its densification strain within this time frame the test

remains incomplete [76]. As the results in Figure 14a indicate that a maximum strain of only approximately 10% was obtained, only the peak strength is examined in detail in this work. Large variation is observed in the measured peak strength under high strain rates, however despite this large variation, the peak strength remains essentially constant when compared in the strain rate range from 10^{-3} /s to 726 /s. An example of the fractured specimens tested at strain rates of 547/s and 648/s are shown in Figure 14b along with an SEM image of a crack bisecting a SiC sphere. Little difference was observed in the macroscopic appearance of specimens tested at higher strain rates, however increased crushing of spheres was observed.

A strain rate sensitivity parameter Σ has been employed by others [73] to identify strengthening phenomena in the case of high strain rate deformation as defined by the following equation:

$$\Sigma = \frac{\sigma_d - \sigma_q}{\sigma^*} \frac{1}{\ln\left(\dot{\varepsilon}_d / \dot{\varepsilon}_q\right)} \qquad (1)$$

where σ is the stress at a given strain, σ^* is the stress at a given strain at a reference strain rate of 10^{-3} s^{-1}, $\dot{\varepsilon}$ is the strain rate, and the subscripts *d* and *q* refer to dynamic and quasi-static testing respectively.

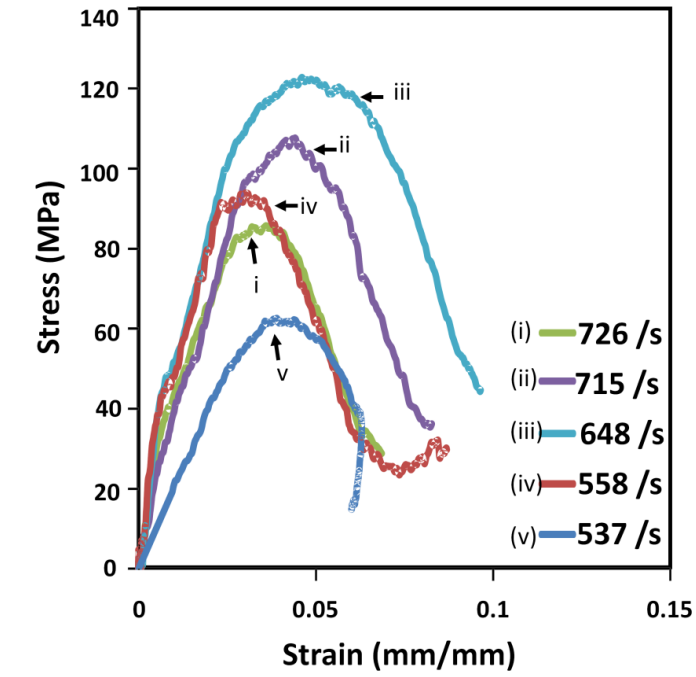

a

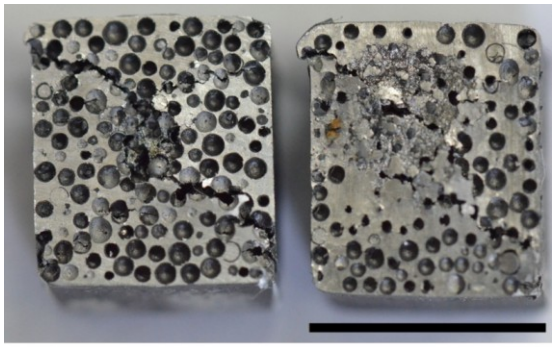

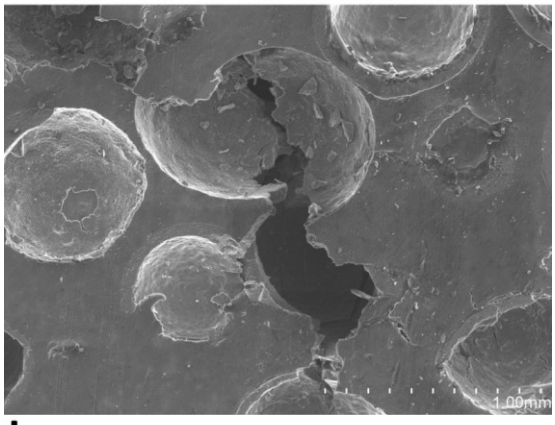

b

FIG. 14. a) High strain rate compression response of Mg-AZ91/SiC syntactic foams. b) Fractured specimens compressed at high strain rates. The top images show fractured specimen tested at strain rates of (from left to right) 537/s and 648/s respectively.

Load was applied on the face that is visible in the image, causing compression through the thickness of the specimen imaged. The lower image shows a typical fracture event in the 537/s specimen where a crack is shown to shear a SiC hollow sphere. Higher strain rates led to increased crushing of the spheres.

The peak stress was used for the dynamic, quasi-static and reference stresses after the analysis of Balch et al. [4] due to the unique deformation behavior of metal foams in comparison to alloys or composites. The calculated sensitivity parameter for these composites was approximately 0.01 or less, which is expected for cellular AZ91 [75] at similar strain rates, leading to the conclusion that the strain rate sensitivity in the case of the Mg-AZ91-SiC syntactic foams is primarily dependent on the matrix properties and not greatly affected by the presence of the SiC hollow spheres within the range of strain rates investigated in this study.

5. Comparison with other Syntactic Foams

Figure 15 shows the Ashby plot of the specific plateau strength vs. the specific energy absorption for aluminum open-celled and syntactic foams available in literature including the data in this study. The performance of the Al-A206 and the Mg-AZ91 syntactic foams, showed improved performance when compared to other similar foams on a specific property basis. A further increase in the performance might be achieved through careful control of the SiC t/D ratio.

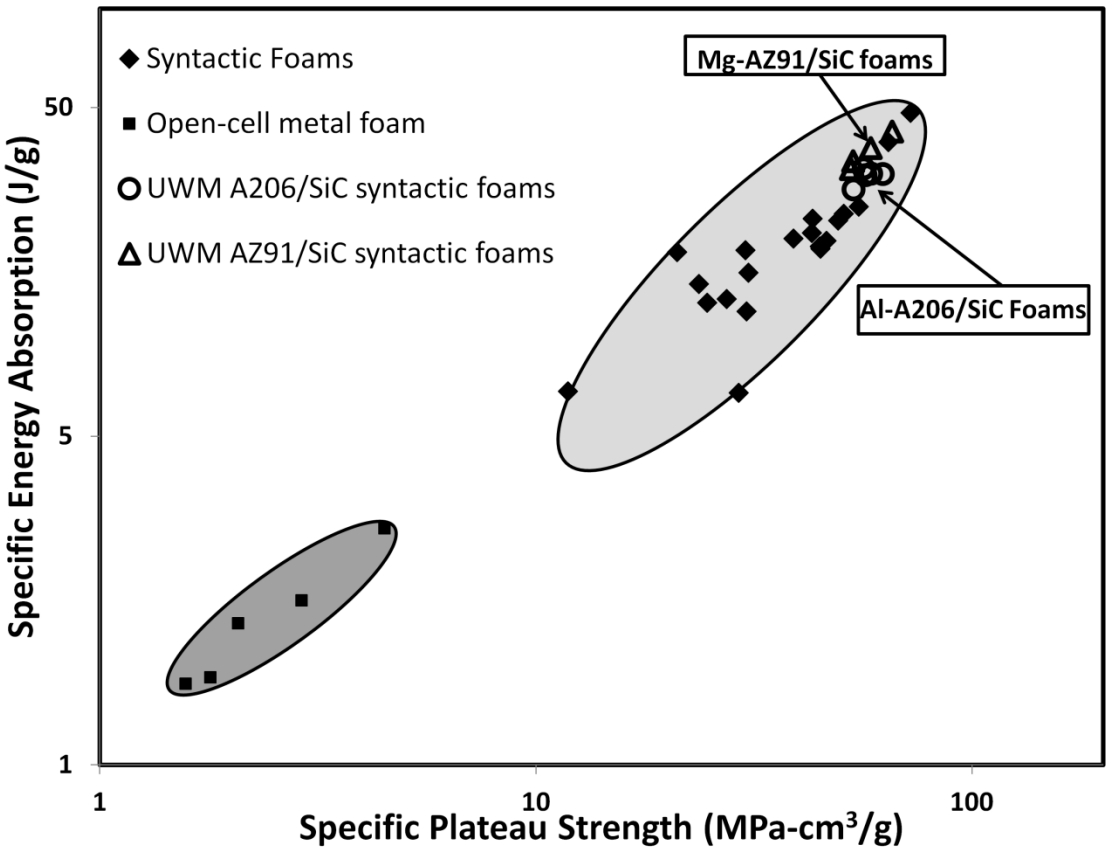

FIG. 15. Log-log plot of specific plateau strength vs. specific energy absorption for different types of aluminum foams [4, 13, 17, 26, 35-37, 46-49, 55].

6. Conclusions

The conclusions of this study can be summarized as:

- The microstructure and quasi-static properties of Al-A206/SiC and Mg-AZ91/SiC hollow sphere syntactic foams have been studied to determine the effect of matrix strength.
- Microstructure of Al-A206 syntactic foams revealed the presence of interdentritic phases containing iron, presumably from the dissolution of iron from the mold during processing. The heat treatments applied, partially dissolved and precipitated the intermetallic network formed.
- Microstructure of Mg-AZ91/SiC syntactic foam showed some refinement in comparison to the matrix alloy, likely due to the restricted solidification of the liquid in spaces between spheres. No evidence of iron inside the matrix was found.
- The peak strength, plateau strength and toughness of the foams increase with increasing yield stress of the matrix material. The increments for the peak stress were 13% for T4 and 24% for T7 treatments, referred to the as cast condition. For the same heat treatments, the increments for the plateau stress were 27% and 37%, while for the Toughness the values were 17% and 26% respectively.
- The Al-A206/SiC and Mg-AZ91/SiC syntactic foams synthesized in this study exhibited a higher specific plateau strength and specific energy absorption than many of the syntactic foams reported in literature, leading to insights regarding

how the properties of metal matrix syntactic foams may be optimized. Strengthening of the matrix proved to be an effective way to enhance the specific properties of the syntactic foams studied.

- The high strain rate properties of the Mg-AZ91/SiC foams were studied in the range of 530 /s to 726 /s, and in this range the sensitivity parameter was less than 0.01 [73]. Therefore, it is concluded that under the conditions studied, there is no strain rate dependence in the peak stress.

7. Future Work

Considering that the syntactic foams synthesized in this study exhibited a higher specific plateau strength and specific energy absorption than many of the syntactic foams reported in literature, future work in the study of SiC metal matrix syntactic foams should include the effect of the t/D ratio on these parameters. Previous studies have shown a close relationship between this ratio and the mechanical performance of MMSF during quasi-static compression tests. The effect of a stronger matrix via heat treatment or other strengthening mechanism should be also studied as well as the synthesis of foams made with smaller microspheres having tighter size ranges. Results reported in the literature, have shown the incorporation of microspheres with these characteristics into a syntactic foam system will increase the peak stress, plateau stress, and toughness.

Development of preforms made from hollow spheres to be infiltrated by the metallic melt is another important area of future work in this field. Although this technique has been widely used for the processing of composites with solid particles and fibers; hollow spheres present a particular restriction, as pressure applied during compacting should be low enough to avoid crushing of the spheres before the foam is synthesized. The use of preforms will maximize the volume percentage of hollow spheres in the foam and will allow the introduction of bimodal distributions of hollow spheres in the foams.

Future work should also be done on the standardization of compression tests, specific for metal matrix syntactic foams, in this way a consistent comparison among results of

different studies will be possible. Currently, there is one international standard (ISO 13314:2011) and several national standards (German, Japanese, British, etc.) for quasi-static compression tests of porous and cellular metals.

Metal matrix syntactic foams are designed to work under compression, especially during impact and blasting. Although this property has been widely studied, there is still controversy upon which type of compression test should better represent the compressive properties of these materials (low, high or intermediate strain rate). It is recommended to complement quasi-static compression tests with high strain rate tests, which seem to represent more closely the behavior of metal matrix syntactic foams in service. Currently, there is one international draft standard (ISO DIS 17340:2013) for high speed compression tests of porous and cellular metals.

8. References

1. Schultz B, Rohatgi P, Metal Matrix Syntactic Foam: Processing, microstructure, properties, applications. Chapter 3, ed. Gupta N, Rohatgi P (in Press, Elsevier); 2013.

2. Rohatgi PK, Guo RQ, Iksan H, Borchelt EJ, Asthana R. Mater. Sci. Eng. A. 1998; 244:22-30.

3. Rohatgi P, Kim J, Gupta N, Alaraj S, Daoud A. Composites Part A. 2006; 47:430-7.
4. Balch DK, O'Dwyer JG, Davis GR, Cady CM, Gray III GT, Dunand D.C. Mater. Sci. Eng. A. 2005; 391:408-17.
5. Orbulov I, Dobránsky J. Period. Polytech. Mech Eng. 2008; 52:35-42.
6. Orbulov I, Gunsztler J. Composites Part A. 2012; 43:553-61.
7. Palmer RA, Gao K, Doan TM, Green L, Cavallaro G. Mater. Sci. Eng. A. 2007; 464:85-92.

8. Drury WJ, Rickles SA, Sanders Jr. TH, Cochran JK. In: Lee EW, Chia EH, Kim NJ. (Eds.) Light-Weight Alloys for Aerospace Applications TMS 1989 pp. 311-22.

9. Kiser M, He MY, Zok FW. Acta Mater. 1999; 47:2685-94.
10. Aghajanian M, Mamillan N, Kennedy C, Luszcz S, Roy R. Mat. Sci. 1989; 24:658-70.
11. Weise J, Yezerska O, Busse M, Haesche M, Zanetti-Bueckmann V, Schmitt M. Materialwiss. Werkstofftech. 2007; 38:901-6.

12. Lanning BR, Rawal SP, Misra MS. in Advanced Metal Matrix Composites for Elevated Temperatures Conference Proceedings, Cincinnati, Ohio October 20-24 1991, pp. 79-83.

13. Rabiei A, Vendra LJ. Mater Lett. 2009; 63:533-6.

14. Zhang LP, Zhao YY. J Composite Mater. 2007; 41:2105-17.

15. Zhao Y, Tao X, Xue X. Proc. MS&T Pittsburgh Pennsylvania. 2008 pp. 2607- 2615.

16. Tao XF, Zhang LP, Zhao YY. Mater Des. 2009; 30:2732-6.

17. Tao XF, Zhao YY. Scr. Mater. 2009; 61:461-4.

18. Kim HS, Plubrai P. Composites Part A. 2004; 35:1009-15.

19. Santa Maria J, Thesis for Master of Science in Engineering at University of Wisconsin-Milwaukee, May 2012.

20. Santa Maria J, Schultz B, Ferguson J, Rohatgi P. DOI 10.1016/jsmea.2013.05.081.

21. Daoud A, Abou El-Khair MT, Abdel-Aziz M, Rohatgi P. Compos. Sci Technol. 2007; 67:1842-53.

22. Daoud A. Mater Sci Eng A. 2008; 488:281-95.

23. Nagata S, Matsuda K. Imono. 1981; 53:300-4.

24. Nagata S, Matsuda K. Jpn. Foundrymen's Soc. 1983; 2:616-20.

25. Mondal DP, Datta Majumder J, Jha N, Badkul A, Das S, Patel A, Gupta G. Mater Des. 2012; 34:82-9

26. Neville BP, Rabiei A. Mater Des. 2008; 29:388-96.

27. Balch DK, Dunand DC. Acta Mater 2006; 54:1501.

28. Weise J, Baumeister J, Yezerska O, Salk N, Silva GBD. Adv. Eng. Mater. 2010; 12:604-8.

29. Peroni L, Scapin M, Avalle M, Weise J, Lehmhus D, Baumeister J, Busse M. Adv. Eng. Mater. 2012; 14:909-18.

30. Peroni L, Scapin M, Avalle M, Weise J, Lehmhus D. Mater Sci Eng A 2012; 552:364-75.

31. Rohatgi PK, Kim JK, Gupta N, Alaraj S, Daoud A. Composites Part A 2006; 37:430.

32. DeFouw JD, Rohatgi PK. Supplemental Proceedings, Vol 2: The Minerals, Metals and Materials Society, Warrendale, PA, 2011, p.797.

33. Castro G, Nutt SR. Mater Sci Eng A 2012; 535:274.

34. Luong DD, Strbik III OM, Hammond VH, Gupta N, and Cho K. J. Alloys Compd. 550, 412 (2013).

35. Wu GH, Dou ZY, Sun DL, Jiang LT, Ding BS, He BF. Scr Mater 2007; 56:221.

36. Vendra LJ, Rabiei A. Mater Sci Eng A 465 (2007) 59–67.

37. Daoud A. J Alloys Compd. 2009; 487:618.

38. Mortensen A, Jin I. Int. Mater. Rev. 37, 101 (1992).

39. Chandler H, ed. Heat Treater's Guide, ASM International 1996, pp.135-145.

40. Talamantes-Silva M, Rodríguez A, Talamantes-Silva J, Valtierra S, Colás R. Metall. Mater Trans B. 39, 911 (2008).

41. Bäckerud L, Chai GJ. Tamminen J. Solidification Characteristics of Aluminum Alloys vol. 2, AFS 1990, pp. 63-69.

42. Srinivasa A, Swaminathan J, Gunjan M, U. Pillai U, Pai B. Mater. Sci. Eng. A. 527, 1395 (2010).

43. Braszczyńska-Malik KN, and Zyska A. Arch. Foundry Eng. 10, 23 (2010).

44. Ureña A, Gómez de Salazar JM, Gil L, Escalera M, Baldonedo JL. J. Microsc. 196, 124 (1999).

45. Luo A. Metall. Mater. Trans. A. 26, 2445 (1995).

46. Dou ZY, Jiang LT,Wu GH, Zhang Q, Xiu ZY, Chen GQ. Scr. Mater. 57, 945 (2007).

47. Feng Y, Tao N, Zhu Z, S. Hu S, and Pan Y. Mater.Lett. 57, 4058 (2003).

48. Kanahashi H, Mukai T, Yamada Y, Shimojima K, Mabuchi M, Aizawa T, Higashi K. Mater. Sci. Eng. A. 308, 283 (2001).

49. Yamada Y, Shimojima K, Sakaguchi Y, Mabuchi M, Nakamura M, Asahina T, Mukai T, Kanahashi H, Higashi K. J. Mater. Sci. Lett. 18, 1477 (1999).

50. Kaufman JG and Rooy EL: Aluminum Alloy Castings: Properties, Processes, and Applications. (ASM International, Materials Park, OH, 2004), pp. 81-82.

51. Kaufman JG: Magnesium Alloy Database (Knovel, Norwich, NY, 2011) Table 2b, Online version available at: http://www.knovel.com/web/portal/browse/display?_EXT_KNOVEL_DISPLAY_bookid=4259&VerticalID=0

52. Gladysz GM, Chawla KK, Boccaccini AR. J Mater Sci (2012) 47:5625–5626

53. Metal Matrix Composites: The Global Market. Website accessed: 2-19-2013 http://www.bccresearch.com/report/metal-matrix-composites-market-avm012d.html

54. Withers G. ULTALITE® aluminum composites, Adv. Mater. Proc. 2005; 163:45-8

55. Zhang Q, Lee PD, Singh R, Wu G, and Lindley TC. Acta Mater. 2009; 57:3003–11

56. Niebylski LM, Fanning RJ. SAE Transactions. Paper 720490, 1972, doi: 10.4271/720490.

57. Rohatgi PK, Gupta N, Schultz BF, Luong DD. JOM. 2011; 63:30-6

58. Kremer K. Final Report IDEA Programs, Transportation Research Board 2004; 34:1-31

59. Read S. Aerofoil and a Method of Manufacturing, Patent No. US 7594325 B2 9-29- 2009

60. Powdermet Inc. Products SCOMP™ Website accessed: 2-19-2013 http://www.powdermetinc.com/scomp.html

61. Chin ESC. Army Mater. Sci. Eng. A. 1999; 259:155-61.

62. Hogg PJ. Composites in Armor, Science. 2006; 314:1100-1.

63. Hou W, Zhu F, Lu G, Fang DN. Int. J Impact Eng. 2010; 37:1045-55.

64. Gama BA, Bogetti TA, Fink BK, Yu CJ, Claar TD, Eifert HH, Gillespie JW. Compos. Struct. 2001; 52:381-95.

65. Rawal SP, Lanning BR. DARPA Report 1994.

66. Mouritz AP, Gellert E, Burchill P, Challis K. Compos. Struct. 2001; 53:21-41.

67. Ridzwan MIZ, Shuib S, Hassan AY, Shokri AA. J. Appl. Sci. 2006; 6:183-9.

68. Soininvaara TA, Jurvelin JS, Miettinen HJA, Suomalainen OT, Alhava EM, Kröger PJ. Calcif. Tissue Int. 2002; 71:472-7.

69. Xue XB, Zhao YY, Kearns V, Williams RL. Supplemental Proceedings: Vol 2: Materials Characterization, Computation, Modeling and Energy. TMS 2010.

70. Salimon A, Bréchet Y, Ashby MF, Greer AL. J. Mater. Sci. 2005; 40:5793-9.

71. Banhart J. Prog. Mater. Sci. 2001; 46:559-632.

72. Dou Z, Wu G, Huang X, Sun D, Jiang L. Composites Part A. 2007; 38:186-91.

73. San Marchi C, Cao F, Kouzeli M, Mortensen A. Mater. Sci. Eng. A. 337, 202 (2002).

74. Ishikawa K, Watanabe H, Mukai T. Mater. Lett. 59, 1511 (2005).

75. Mukai T, Kanahashi H, Yamada Y, Shimojima K, Mabuchi M, Nieh TG, Higashi K. Scr. Mater. 41, 365 (1999).

76. Gupta N, Luong DD, and Rohatgi PK. J. Appl. Phys. 109, 103512 (2011).

77. Chawla K. Composite Materials: Science and Engineering, 3rd Ed., Springer.